

Published in final edited form as:

Biomacromolecules. 2011 May 9; 12(5): 1675–1685. doi:10.1021/bm2000605.

AFM study of morphology and mechanical properties of a chimeric spider silk and bone sialoprotein protein for bone regeneration

Sílvia Gomes^{1,2,3}, Keiji Numata⁴, Isabel B. Leonor^{1,2}, João F. Mano^{1,2}, Rui L. Reis^{1,2,*}, and David L. Kaplan^{3,*}

Sílvia Gomes: silvia.gomes@dep.uminho.pt; Keiji Numata: keiji.numata@riken.jp; Isabel B. Leonor: belinha@dep.uminho.pt; João F. Mano: jmano@dep.uminho.pt; Rui L. Reis: rgreis@dep.uminho.pt; David L. Kaplan: David.Kaplan@tufts.edu

¹ 3B's Research Group - Biomaterials, Biodegradables and Biomimetics, Department of Polymer Engineering, University of Minho, Headquarters of the European Institute of Excellence on Tissue Engineering and Regenerative Medicine, AvePark, Zona Industrial da Gandra 4806-909 Caldas das Taipas, Guimarães, Portugal

² Institute for Biotechnology and Bioengineering (IBB), PT Associated Laboratory, Braga, Portugal

³ Departments of Biomedical Engineering, Tufts University, Medford, Massachusetts 02155 USA

⁴ Enzyme Research Team, Biomass Engineering Program, RIKEN, 2-1 Hirosawa, Wako-shi, Saitama, 351-0198, Japan

Abstract

Atomic force microscopy (AFM) was used to assess a new chimeric protein consisting of a fusion protein of the consensus repeat for *Nephila clavipes* spider dragline protein and bone sialoprotein (6mer+BSP). The elastic modulus of this protein in film form was assessed through force curves, and film surface roughness was also determined. The results showed a significant difference between the elastic modulus of the chimeric silk protein, 6mer+BSP, and control films consisting of only the silk component (6mer). The behaviour of the 6mer+BSP and 6mer proteins in aqueous solution in the presence of calcium (Ca) ions was also assessed to determine interactions between the inorganic and organic components related to bone interactions, anchoring and biomaterial network formation. The results demonstrated the formation of protein networks in the presence of Ca²⁺ ions, characteristics that may be important in the context of controlling materials assembly and properties related to bone-formation with this new chimeric silk-BSP protein.

Keywords

Atomic force microscope; chimeric proteins; silk; mechanical properties; calcium mediated networks; bone regeneration

1. Introduction

With the potential importance of tissue engineering in healthcare the design of new biopolymers with improved mechanical and biocompatibility characteristics has become a

*CORRESPONDING AUTHOR FOOTNOTE: David L. Kaplan: David.Kaplan@tufts.edu, Tufts University, 4 Street, Medford, MA 02155, Tel: 617-627-3251, Fax: 617-627-3231. Rui L. Reis^{1, 2}: rgreis@dep.uminho.pt, 3B's Research Group - Biomaterials, Biodegradables and Biomimetics, Department of Polymer Engineering, University of Minho, AvePark, Zona Industrial da Gandra 4806-909 Caldas das Taipas, Guimarães, Portugal.

major goal in the field of biomaterials research. Spider dragline silk fibers exhibit remarkable viscoelastic properties, combining a tensile strength similar to steel and Kevlar with a high elasticity that is comparable to rubber¹. In part these mechanical properties are a consequence of the amino acid chemistry where the hydrophilic GGX motif (G stands for glycine, X is mostly glutamine) alternates with poly-alanine (poly-A) motifs². The GGX motif adopts a helical conformation forming an amorphous region that connects the poly-A motifs, providing elasticity to the silk fiber. The hydrophobic poly-A motifs are responsible for the formation of rigid and highly packed anti-parallel β sheets³ resulting from hydrogen bonding and hydrophobic interactions⁴. The remarkable mechanical properties together with the inherent biocompatibility suggest spider silk as a promising biopolymer for bone repairs and bone growth⁵. Recently, a spider protein inspired by dragline silk from *Euprosthenois australis* was expressed in *Escherichia coli* and used to produce meter-long fibers with a tensile strength of approximately 0.2 GPa, which is above the values for mammalian bone and tendon^{6, 7}, and a elastic modulus of 7 GPa, comparable to native dragline from *Nephila clavipes*⁸. Furthermore, *in vitro* tests with HEK 293 cells indicated that these fibers were biocompatible and capable of sustaining cell attachment and growth⁸.

Recombinant spider silk offers advantages over natural spider silk. With recombinant DNA technology the protein amino acid sequence and length can be controlled to tailor the sequence chemistry and polymer features to the target needs in terms of structure and functional features^{9, 10}. Our previous work¹¹ described the synthesis of a new chimeric protein through the fusion of a spider silk (6mer) with six repeats of the consensus amino acid block from the native sequence of the major ampullate dragline silk I protein, MaSpI, from the spider specie *Nephila clavipes*, with bone sialoprotein sequence (BSP) designated by 6mer+BSP (Figure 1). BSP is a noncollagenous protein present in bone tissue that can induce the deposition of calcium phosphate in the form of hydroxyapatite and bind to collagen fibers¹². At the cellular level BSP induces the attachment and differentiation of osteoblasts¹³ and stimulates osteoclast activity¹⁴, thereby playing an important part in the remodelling process of bone. In previous work we demonstrated that the fusion protein 6mer+BSP maintains the ability to induce the deposition of calcium phosphate, due to the presence of the BSP domain¹¹.

In the present study atomic force microscopy (AFM) was used to collect topographic images of 6mer and 6mer+BSP films, to measure surface roughness of these films and to assess the elasticity of the films, since AFM can also be used to determine local mechanical properties of soft polymeric samples¹⁵. The AFM tip is used to indent the sample resulting in a force curve that can be analyzed for elastic response of the sample to the small loading force applied by the tip¹⁵. The Hertz model for elastic indentations can be used to calculate Young's modulus (E)¹⁶. Previous studies have used AFM to measure the elastic properties of spider silk either by stretching a spider silk fiber attached to the AFM tip⁹ or by indentation into the fiber¹⁶. In the present work, AFM was used to assess the elasticity of 6mer+BSP films vs. the controls.

Since 6mer+BSP was synthesized for bone-related biomaterial needs, the behaviour of 6mer+BSP in the presence of divalent Ca^{2+} was also assessed with AFM imaging. The deposition of calcium phosphate induced by BSP is related to the negatively charged polyglutamic sequences that interact with positively charged Ca^{2+} ions^{17, 18}. The binding with Ca^{2+} ions was important in the formation of Ca mediated networks of osteopontin proteins, increasing the ability of these networks to dissipate energy in response to applied forces, contributing to bone plasticity¹⁹. The study of 6mer+BSP in the presence of Ca^{2+} ions is important to gain insight into how these types of molecules form Ca mediated networks related to bone regeneration. The presence of these types of Ca-BSP networks fully integrated with a robust silk biomaterial could be useful both in osteointegration as well as for structural support.

2. Materials and Methods

2.1. Cloning and protein expression

The clone carrying the DNA sequence coding for BSP was purchased from the Harvard clone collection (Clone Identification: HsCD00082642, “The ORFeome Collaboration” Dana-Farber/Harvard Cancer Center, Boston, MA, USA) and inserted in the vector pET30L (Novagen, San Diego, CA, USA) carrying the silk block copolymer¹⁰, as we have described previously¹¹. The 6mer+BSP protein was expressed in *E. coli* RY-3041 strain grown in Hyper Broth™ (0107-S, Athens Enzyme Systems, Baltimore, MD, USA) to an OD₆₀₀ of 1 in the presence of kanamycin 25 µg/ml. Expression was induced with isopropyl β-D-thiogalactoside (IPTG, 15529019, Invitrogen, Carlsbad, CA, USA) 0.5 mM. The cells were harvested by centrifugation and cell pellet was lysed under denaturing conditions using the buffer 100 mM NaH₂PO₄, 10 mM Tris HCl, 8 M urea (pH 8.0). Insoluble cell debris was excluded from the mixture by centrifugation and the supernatant was collected. After incubating the supernatant with Ni-NTA resin (30250, Qiagen, Valencia, CA, USA) for two hours, the mixture was loaded in a column and washed several times with denaturing buffer at pH 8 and at pH 6.0. Protein was eluted using denaturing buffer at pH 4.5. Protein solution was loaded into snake skin membranes (131054, Spectra/por Biotech, Rancho Dominguez, CA, USA) and dialysed against 20 mM sodium acetate buffer (pH 4.75) followed by dialysis in MQ water. Finally protein solution was lyophilized in a LabConco (Kansas city, MO, USA) lyophilizer.

2.2. Sample preparation

The 6mer+BSP and 6mer protein (silk control) were dissolved in MQ water to a final concentration of 2% (m/v). Then 20 µl of protein solution was cast onto freshly cleaved mica surfaces and left to dry at room temperature. After drying the protein films were treated with 70% methanol solution for two hours to induce the transition of secondary structure from random coil to β-sheet, providing stability in aqueous solutions. A total of three protein films were used to collect force curves. To study the formation of protein networks, the 6mer+BSP and 6mer proteins were dissolved in three different solutions: 4-(2-hydroxyethyl)-1-piperazineethanesulfonic acid (HEPES, pH 7.4) 0.1 mM buffer, HEPES 0.1 mM buffer containing magnesium (Mg⁺²) ions in a molar ratio of 1:1000 (protein:Mg) and HEPES 0.1 mM buffer containing Ca²⁺ ions in a molar ratio of 1:1000 (protein:Ca)²⁰. The final protein concentration was 0.01 mg/ml. Protein solution was deposited onto a freshly cleaved mica surfaces and left to dry at room temperature.

2.3. AFM imaging and force spectroscopy

An AFM (Veeco Dimension V 3100 Scanning Probe Microscope, NY, USA) with a scanning range of 90 µm² and a z range of 7–8 µm was used for imaging and force-curve measurements. AFM cantilevers (Veeco, FESP) made of silicon with a spring constant of 3.152 N/m were used and AFM imaging and force-curve measurements were performed in the dry mode. A total of 100 force curves were recorded for both 6mer+BSP and 6mer films, respectively, using the software NanoScope V (Veeco). Mica was used as a control. Force curves were collected using contact mode AFM. Samples were imaged with tapping mode AFM. The tapping mode operation allowed the visualization of weakly adsorbed samples by eliminating the lateral forces between the probe tip and the sample²¹. The heights of the structures imaged on mica were determined by section analysis using Nanoscope image analysis software. Roughness measurements were performed with the NanoScope V (Veeco). Two values were measured: the root mean square (RMS) and the arithmetic average height (R_a). RMS represents the standard deviation of the height values within a given area and allows the surface roughness to be determined by statistical methods^{22, 23}. R_a is the most frequently used roughness parameter and is defined as the average deviation of

the roughness irregularities from the mean line over one sampling length^{22, 23}. Because roughness values change with the scan size the measurements were performed using three different scan windows: $20 \times 20 \mu\text{m}^2$, $10 \times 10 \mu\text{m}^2$ and $2 \times 2 \mu\text{m}^2$.

2.4. Analysis of the data from the force curve measurements

In a force curve, the cantilever deflection (d) is registered as a function of its vertical position (z) [equation 1 (Eq. 1)]. The slope of the force curve gives a qualitative idea of the sample elastic properties. For a stiff sample the force curve is characterized by a flat area when the tip is approaching the sample and by a slope region where the cantilever deflection is identical to the z movement, $d = z$ ^{15, 16}. However, in the case of a soft sample this slope region becomes shallower as a result of the decrease in the deflection value due to elastic indentation (δ),

$$d = z - \delta \quad (\text{Eq. 1})$$

Hooke's law relates the deflection with the applied force through the force constant of the cantilever (k)

$$F = kd = k(z - \delta) \quad (\text{Eq. 2})$$

The Hertz model relates the indentation δ with the loading force F and by using the Sneddon modification^{24, 25} we have

$$F = \frac{2}{\pi} \cdot \frac{E}{1 - \nu^2} \cdot \delta^2 \cdot \tan(\alpha) \quad (\text{Eq. 3})$$

where E is the elastic or Young's modulus, ν is the Poisson ration of the sample, assumed to be 0.5 for incompressible materials²⁶, and α is the opening angle of the AFM tip. By combining equations 2 and 3 we have

$$kd = \frac{2}{\pi} \cdot \frac{E}{1 - \nu^2} \cdot \delta^2 \cdot \tan(\alpha) \quad (\text{Eq. 4})$$

Whit the rearrangement of equation 3 we have an expression for indentation δ

$$\delta = \sqrt{\frac{kd}{(2/\pi)[E/(1 - \nu^2)]\tan(\alpha)}} \quad (\text{Eq. 5})$$

Since δ can not be detected directly by AFM it can be replaced by combining equations 1 and 5²⁷

$$z=d+\sqrt{\frac{kd}{(2/\pi)[E/(1-v^2)]\tan(\alpha)}} \quad (\text{Eq. 6})$$

For data treatment we will use the more general form

$$|z-z_0|=d-d_0+\sqrt{\frac{k(d-d_0)}{(2/\pi)[E/(1-v^2)]\tan(\alpha)}} \quad (\text{Eq. 7})$$

d_0 and z_0 are the initial values of deflection and height, respectively²⁸.

Equation 7 was used to fit the data from the recorded force curves and to calculate the value of the elastic modulus, E , for the 6mer+BSP and 6mer films.

2.5. Secondary structure analysis

Since β -sheet and random coil/helix content are considered major factors related to the mechanical properties of spider silk materials, Attenuated-Total Reflectance Fourier Transform Infrared Spectroscopy (ATR-FTIR) was performed to assess the secondary conformation of both the 6mer and 6mer+BSP proteins. These data provide structural details to support the interpretation of mechanical properties from the AFM studies, including the differences between the calculated Young's modulus for the 6mer and 6mer+BSP films. ATR-FTIR measurements were performed with the 6mer and 6mer+BSP films, prepared as mentioned in section 2.2, using a Jasco model FT/IR-6200 type A equipment (Jasco Inc. MD, USA). Spectra were collected in absorption mode at 8 cm^{-1} resolution using 64 scans in the spectral range 4000 to 400 cm^{-1} . The quantification of secondary structure was based on the analysis of the amide I region (1700 to 1600 cm^{-1}) and was determined through the deconvolution of the spectra followed by the normalization of the obtained values to the total area of the amide I region²⁹. Briefly, OPUS deconvolution software (Bruker optics, Billerica, MA, USA) was used for spectra deconvolution. Following deconvolution the spectra were curve-fitted with Gaussian bands using the peak pick function and the information concerning the percentage of amide I and II regions, bandwidth and band position, referring to β -sheet or α -helix conformations, can be obtained³⁰.

2.6. Circular dichroism

Circular dichroism (CD) spectroscopy was performed with an Aviv, Model 410 (Biomedical, Inc. NJ USA) equipment. The spectra were collected between 260 and 180 nm with a step size of 1 nm , an averaging time of 1 s . A total of five scans were collected in three different samples for each condition. A baseline spectrum was subtracted from the samples. Cells of 0.1 cm path length were used and measurements were performed with 1 mg/ml protein solutions in 0.1 mM HEPES buffer ($\text{pH } 7.4$) and in 0.1 mM HEPES containing Ca^{2+} ions in a molar ratio of $1:1000$ (protein:Ca), as mentioned in section 2.2. The procedure was repeated in the presence of Mg^{2+} ions, 0.1 mM HEPES containing Mg^{2+} ions in a molar ratio of $1:1000$ (protein:Mg). CD provided a check to determine if there were any differences in secondary conformation of the 6mer+BSP and 6mer when in a buffer solution with pH of 7.4 in the presence of Ca^{2+} or Mg^{2+} ions.

2.7. Statistical analysis

Statistical analysis was performed with SPSS 17.0. Shapiro-Wilk test was used to test for the normality of the data. Because the data had no normal distribution, the nonparametric Mann-Whitney test was used to test for significant differences. In the case of data with normal distribution the parametric test *t* was used. Statistical significance was defined as $p < 0.05$.

3. Results

3.1. Force curves and Young's modulus (*E*) calculations

Figure 2 shows the force curves for the 6mer and 6mer+BSP films and on a hard sample control, mica. By comparing the slope regions the elastic modulus (*E*) was calculated using the *d* and *z* values extracted from the force curves collected using equation 7 (2.4. Materials and Methods section). The *E* values for both the 6mer and 6mer+BSP films were 1.1 ± 0.6 GPa and 1.5 ± 0.6 GPa, respectively, and were calculated based on the force curves collected for at least 100 different points in each protein film. Statistical analysis indicated that the Young's modulus value calculated for the 6mer film was significantly lower than the value obtained for the 6mer+BSP film ($p < 0.05$). *E* values were calculated by averaging over all points where the force curves were collected.

3.2. Secondary structure analysis

For both the protein films, 6mer control and 6mer+BSP, ATR-FTIR spectra revealed no major differences between secondary structures. For both proteins two peaks were observed, at 1624 and 1520 cm^{-1} , indicative of an antiparallel β -sheet conformation, and a third peak was found at 1650 cm^{-1} corresponding to a helix/random coil conformation^{2, 10, 31} (Figure 3). Spectral deconvolution indicated that both proteins had similar percentages of β -sheet and helix/random coil (Table 1) and statistical analysis indicated no significant difference ($p > 0.05$).

3.3. Roughness measurements

Figure 4 shows representative surface topographies from AFM images of the 6mer and 6mer+BSP films, used for the calculation of the roughness values RMS and R_a . RMS and R_a values were similar for the 6mer and 6mer+BSP films (Table 2) and statistical comparison indicated no significant difference ($p > 0.05$). The RMS value for blank mica using the scan sizes of $20 \times 20 \mu\text{m}^2$, $10 \times 10 \mu\text{m}^2$, $2 \times 2 \mu\text{m}^2$ were 0.881 , 0.455 and 0.085 nm, respectively. For R_a these values were 0.712 , 0.377 and 0.067 nm for $20 \times 20 \mu\text{m}^2$, $10 \times 10 \mu\text{m}^2$ and $2 \times 2 \mu\text{m}^2$ scan sizes, respectively.

3.4. AFM imaging

Tapping mode AFM imaging showed that when dissolved in HEPES 0.1 mM ($\text{pH } 7.4$) most of the 6mer appeared as large globular, amorphous protein aggregates (Figure 5A). The aggregates had different sizes, with diameters ranging from 0.489 to $0.736 \mu\text{m}$ and heights varying from 122.7 to 134.7 nm. Aggregates with similar morphology and size were also observed when the 6mer protein was dissolved in HEPES buffer containing Mg^{2+} ions in a molar ratio of $1:1000$, protein:Mg (Figure 6A). However, after dissolving the 6mer protein in HEPES buffer containing Ca^{2+} ions in a molar ratio of $1:1000$ (protein:Ca) the 6mer appeared more fibrous with a tendency to form fiber aggregates (Figure 7A). The cross-sections of these fibers or aggregates showed a width ranging from approximately 0.1 to $0.04 \mu\text{m}$ and a height between 2.6 and 5.8 nm.

In the case of the 6mer+BSP dissolved in HEPES, AFM imaging revealed two different forms of aggregates: elongated sheets forming large assemblies and spherical particles

(Figure 5B). The sheets had heights between 1.4 and 1.8 nm. The second population of aggregates corresponding to spherical particles had heights between 6 and 7 nm (Figure 5B of 6.82 nm) and widths around 0.098 μm . Both types of aggregates had different shapes from those observed in the case of the 6mer protein dissolved in HEPES. Similarly to what happen with the 6mer protein, when the 6mer+BSP was dissolved in HEPES buffer containing Mg^{2+} ions the aggregates observed were similar to those obtained when dissolved in HEPES solution only. Once again large assemblies of elongated sheets were detected together with particles with an amorphous shape. These sheets had heights ranging between 1.89 and 1.35 nm, as observed for the HEPES solution (Figure 6B).

When the 6mer+BSP protein was dissolved in HEPES with Ca two distinct structures were observed, one corresponding to protein networks with different widths and another corresponding to individualized particles (monomers and dimers). The widths for the aggregate networks varied, the smaller ones in Figure 7B1 have widths of around 0.2 nm and the largest ones corresponding to number 3 had diameters of 1.1 nm as seen in cross-sectional images. The height values for these structures were between 1.9 and 2.3 nm. The second population of structures corresponded to particles with diameters of 0.02 to 0.04 μm and heights of around 0.8 nm (see section for Figure 7B3). Once again the forms observed were different from those imaged with the 6mer protein and also different from those detected for the 6mer+BSP dissolved in HEPES and HEPES with Mg added.

3.5. CD analysis

CD spectroscopy for the 6mer protein showed no apparent difference between the spectra collected for the protein dissolved in HEPES and that dissolved in HEPES with Ca or Mg added. For the three spectra a predominance of β -hairpin conformation (Figure 8) was found, characterized by a negative ellipticity with a minimum at approximately 202 $\text{nm}^{32, 33}$. Also for the BSP+6mer protein no major differences were observed between the spectra collected in the presence of Ca or Mg and in HEPES. In the three spectra the presence of α -helix was observed, with two minima at 210 and 220 $\text{nm}^{32, 33}$ (Figure 8).

4. Discussion

In the present work the Young's modulus was calculated for the 6mer control and 6mer+BSP films based in the force curves. The values for the Young's modulus were 1.1 ± 0.6 and 1.5 ± 0.6 GPa for the 6mer and 6mer+BSP films, respectively, and statistical analysis showed a significant difference ($p < 0.05$). This divergence may be due to the insertion of the BSP domain which could interfere with the ability of the silk to form β -strands, resulting in a change in assembly and thus in mechanical characteristics. However, ATR-FTIR analysis showed a similar presence of the β -sheet (1624 and 1520 cm^{-1}) for both the 6mer and 6mer+BSP films, after treatment with methanol. Furthermore, with the deconvolution of ATR-FTIR spectra the percentage of β -sheet and random coil showed no statistical differences ($p > 0.05$) between the 6mer and 6mer+BSP films.

An alternative explanation for the differences in mechanical properties determined by AFM could be the high content of the amino acid glutamic acid in the BSP domain¹⁷ of the 6mer+BSP protein. Mechanical studies performed on silkworm silk fibers treated with four different solvents (water, acetone, ethanol and isopropanol) showed that immersion in acetone, ethanol and isopropanol leads to an increase in stiffness when compared with water. In contrast, the immersion of fibers in water resulted in a decrease in tensile modulus of the fibers. These results were explained by the fact that water disrupts inter- and intra-molecular hydrogen bonding in the silk matrix. This disruption allows the molecules to move with greater freedom resulting in more flexible and elastic fibers³⁴ with a consequent decrease of stiffness, which was also observed for other biopolymers such as chitosan in the presence of

water³⁵. These hydrogen bonds occur between the amide hydrogen and carbonyl oxygen present in adjacent protein chains³⁶. In the 6mer+BSP sequence the carboxyl groups present in the side chains of the glutamic acid residues constitutes an additional hydrogen donor increasing the number of hydrogen bonds occurring between protein chains. Different studies performed with poly-glutamic peptides demonstrate the ability of these molecules to form strong hydrogen bonds^{37, 38}. The presence of several glutamic acid residues with carboxyl groups in their side chains in the BSP sequence may also contribute to an increase in the number hydrogen bonds in the 6mer+BSP proteins¹⁷. This gain in hydrogen bonding between 6mer+BSP proteins chains may be a reason for the higher stiffness observed for 6mer+BSP films when compared with 6mer films. As mentioned above, the increase in number of hydrogen bonds between silk chain segments, as a consequence of the treatment with organic solvents, resulted in an increase in elastic modulus values for silk³⁹.

Furthermore, the values of 1.1 ± 0.6 and 1.5 ± 0.6 GPa obtained for the 6mer and 6mer+BSP films are close to the values obtained for silk fibroin films, 2.7 GPa⁴⁰ but still far from the values of 20–22 GPa for stiffness attributed to the major ampullate dragline silk from the spider *Nephila clavipes*⁴¹. This difference indicates that there remains a lot to learn about processing and assembly of silk proteins related to functional properties. Finally, the elastic behaviour of a protein can also be assessed through AFM force spectroscopy by using the pulling mode. In this mode the cantilever tip is pressed against the molecules deposited on the slide, picking up one or more molecules, which are then stretched between the tip and the slide generating a force versus extension curve⁴². By pulling the protein chain it is possible to measure the force required to unfold domains or loops or to break these molecules. This technique has been applied to different proteins, including silk, showing that in case of elastic fibres the force increases slowly when the fiber is stretched until it reaches its elastic limit, meaning that the pulling force must be applied over larger extensions and increasing the area under the force-extension curve. In the case of stiff materials with small elastic strains, since the extension over which the pulling force must be exerted is smaller, the area under the force-extension curve is smaller⁴³. In this way, AFM force spectroscopy either by pulling mode or by contact mode can be used to assess two different perspectives of the elastic behaviour of a material or protein fiber.

AFM was also used to provide topographic images and roughness for the 6mer and 6mer+BSP films. The topographic images show that the 6mer+BSP films had a smoother surface than the 6mer films, however, a statistical comparison showed no significant difference between. Furthermore, the roughness values indicated a relationship between this parameter and the size of the scanned area; an increase in the size of the scanned area resulted in an increase in roughness values. This phenomenon was observed for both the 6mer and 6mer+BSP films (Table 2). Similar results were obtained in other studies when measuring the roughness properties of different materials using AFM^{44–48}. A possible reason for this result is the effect of tip geometry on the measurements of surface roughness. At small scan sizes, if the tip is larger than the features causing the surface texture the surface will appear flatter as a consequence of poor access to lower points on the surface, and the roughness values will be lower⁴⁸. With the increase of the scan size there is an increase of roughness values⁴⁶. In this way, by changing the scan size it is possible to acquire different surface topographies, with different roughness values⁴⁴. The characterization of material surface roughness at different length scales is important since biocompatibility of a material is dependent on material chemistry and physical features, as well as on surface roughness⁴⁹. Studies indicate that different scales of roughness induce different cell responses. The use of osteoblast-like U-2 OS cells showed that surface roughness of ground titanium had a significant effect on the adhesion of the cells. Cell adhesion and spreading had better outcomes for a roughness of $0.15 \mu\text{m}$ in comparison with smoother (0.05 and $0.07 \mu\text{m}$) or rougher (0.33 and $1.20 \mu\text{m}$) surfaces⁴⁹. Moreover, other studies indicate that roughness is

important in determining cell response as long as roughness can be sensed by cells, meaning that the distance between peaks should not exceed the ability of the cell to form focal attachments in two or more peaks, otherwise the cell will sense the surface as smooth⁵⁰. However, in a study with MG63 cells focal contacts formed more rapidly on smooth nanotopographies than on rougher anodized surfaces⁵¹. Recently, osteoblasts were found to responded better, spreading and forming lamellipodia, to smoother surfaces at microscopic length scales and rougher surfaces at macroscopic length scales⁵². In the same study, results obtained with *Staphylococcus epidermis* indicated that colonization was more effective in surfaces with roughness at the microscopic level⁵². Since micrometer and nanometer scales affect different aspects of cell behaviour and different cell types react differently to surface topography⁵¹ it is important to study the surface roughness over a range of length scales⁵³.

Finally, the behaviour of the 6mer+BSP protein in the presence of divalent ions, Ca^{2+} and Mg^{2+} , was investigated. During the past few years the role of Ca^{2+} ion in the formation of protein networks has been studied due to the importance of these networks in mechanical properties. For example, the abalone shell is a good example of a composite material formed by calcium carbonate plates arranged between organic matrix layers of β -chitin and proteins named lustrins⁵⁴. The organic layers are responsible for the remarkable properties of these natural composites^{43, 54, 55} acting as a organic adhesive holding the calcium carbonate plates together. Smith and co-workers⁴³ used AFM to carry out pulling experiments on freshly cleaved nacre surfaces and obtained force-extension curves with a saw-tooth pattern probably resultant from the repeated unfolding of molecules, such as lustrin A. This unfolding is the outcome of successive opening of folded or looped domains of long molecular chains. When the pulling force rises to a value close to that needed to break the molecule backbone a domain unfolds or a loop opens and the molecule needs to be pulled again until another domain unfolds or a loop opens. Only when all the domains are unfolded and loops opened does the molecule finally break⁴³. Furthermore, when the applied force is relaxed the unfolded domains and open loops have the ability to reform acting as a self-healing mechanism⁴³. These sacrificial bonds are believed to be the key for the outstanding mechanical properties of natural biocomposites^{43, 56}. Divalent ions like Ca^{2+} and Mg^{2+} are crucial for the formation of these sacrificial bonds since this mechanism relies in the formation of intra and inter-chain ionic bond cross-links. Nacre organic matrix is rich in acidic macromolecules in which carboxylate groups are strong Ca binders⁵⁵ and are probably involved in the formation of sacrificial bonds. Other AFM studies performed with the cement tube of *Phragmatopoma californica* worms⁵⁷ and with the cell wall of *Cylindrotheca fusiformis* diatom give similar results⁵⁸.

Bone is also a good example of a natural biocomposite where the formation of Ca mediated sacrificial bonds and the presence of unfolded lengths are responsible for the stiffness and enhanced energy dissipation^{56, 59-63}. The presence of many noncollagenous proteins in bone organic matrix such as bone sialoprotein and osteopontin, in the case of bone, and amelogenin⁶⁴ in the case of dental enamel, with a high number of negatively charged groups are capable of binding together through the formation of Ca ionic bonds⁶³. This organic matrix acts as glue embedding the mineralized collagen fibrils and is capable of dissipating energy through the rupture of sacrificial bonds and stretching molecules, preventing the formation of cracks and increasing the total energy needed to fracture the material, thereby contributing to the improved toughness⁶⁰. As in the case of nacre, when the applied force is removed the sacrificial bonds reform allowing the bone to repair itself⁵⁶.

Because it is still unclear which molecules are involved in the formation of these protein networks and what bonds are responsible for keeping them together some studies addressing the network forming behaviour of different proteins present in tooth and bone organic matrix have been published. Fincham and co-workers studied the self-assembly of a recombinant

amelogenin protein and found that this protein was capable of forming supra-molecular aggregates which the authors suggest to be responsible for controlling the formation of enamel crystals⁶⁴. More recently, a recombinant osteopontin protein was reported to form long aggregate networks and to dissipate large amounts of energy when its molecules were pulled by an AFM cantilever tip¹⁹. In the presence of Ca^{2+} ions the resistance of these protein networks to the pulling force increased considerably¹⁹. The same authors performed similar experiments with other proteins, namely BSP¹⁹ and dentin matrix protein⁶⁵, and the same network-forming tendency was observed. As in the case of osteopontin the presence of Ca potentiated the network-forming behaviour.

In the present work one of the objectives was to study the behaviour of 6mer+BSP protein in the presence of Ca^{2+} ions. In the same way as other negatively charged proteins, osteopontin, BSP, amelogenin and dentin matrix protein, our chimeric silk-BSP protein retained the ability to form supramolecular aggregates and in the presence of Ca^{2+} ions these aggregates generated networks which, as in the case of amelogenin⁶⁴, co-existed with protein monomers and multimers. These structures were not observed in the presence of Mg^{2+} ion which suggests affinity of the BSP domain to Ca^{2+} over other divalent ions as Mg^{2+} . The size of Ca^{2+} ion electron cloud may be the cause for this selectivity⁶⁶.

Furthermore, in the case of the 6mer+BSP protein the network-forming behaviour could be potentiated due to the presence of the spider silk domain (6mer). AFM mechanical and structural studies with a recombinant dragline silk protein showed that this protein spontaneously forms long nanofibers with high intersegment flexibility. When subjected to a pulling force the force vs. piezo extension curves displayed a saw-tooth rupture pattern most probably due to the presence of sacrificial bonds⁹. Similar patterns were obtained with the capture silk fibers from *Araneus*, a orb-weaving spider, where a pulling force revealed rupture peaks due to the break of sacrificial bonds, that reform after relaxation of the fibers⁴². These rupture peaks are also characteristic of the composite materials and proteins mentioned above, placing silk fibers in the category of the self-healing biomaterials⁴². Although we did not observe the formation of nanofibers when the 6mer was dissolved in HEPES alone, the formation of supra-molecular complexes resembling fibers was observed when Ca was added to the HEPES solution. These results are in accordance with the outcomes of other studies where AFM⁶⁷ and dynamic light scattering (DLS)⁶⁸ were used to assess the behaviour of fibroin, from *Bombyx mori*, in the presence of Ca^{2+} ions. In these studies, silk fibroin molecules gave rise to intermolecular networks through the formation of ionic bonds between divalent ions, mainly Ca^{2+} , and the anionic carboxylic groups (COO^-) of fibroin amino acid groups^{67, 68}.

CD spectra indicated that no conformational change was induced by the presence of Ca^{2+} ions, suggesting that the interaction between 6mer+BSP and 6mer and Ca is probably induced by electrostatic attractions rather than by a conformational change in the protein structure⁶⁹. Moreover, there are some differences between the secondary conformations determined by ATR-FTIR and CD for 6mer+BSP and 6mer proteins. These differences are probably due to the different treatments to which samples were subjected before ATR-FTIR and CD analyses. The treatment with methanol removes water molecules from the 6mer+BSP and 6mer films inducing a rearrangement of the hydrogen bonding leading to an increase in the β -sheet content⁶⁷. In the case of CD analysis 6mer+BSP and 6mer proteins were dissolved in a aqueous solution and water molecules disrupt inter- and intra-molecular hydrogen bonding allowing for protein molecules to move with greater freedom and thus forming structures more flexible than β -sheets³⁴. Additionally, different studies show the importance of protein-solvent interactions in protein structure, indicating that protein conformation can change according to the solvent used^{70, 71}. This is likely the case for the differences in the secondary conformations obtained with ATR-FTIR and CD analyses.

As mentioned previously and based on the results obtained by different authors, Ca^{2+} ions seems to be a crucial element for the maintenance of mechanical integrity of many biological systems. The development of new biocomposite materials for biomedical applications is a desired goal. The design of novel organic-inorganic hybrid biomaterials⁷², such as those described in the present work, may provide a new family of high performance structures for bone regeneration. The results discussed above re-enforce the potential of 6mer+BSP proteins in the development of these types of new hybrid biomaterials, where design principles can be employed in specialized designs for structural and functional outcomes.

5. Conclusions

The main goal of the present study was to assess the mechanical and structural characteristics of a new recombinant protein, 6mer+BSP, using AFM for imaging and force spectroscopy. In our previous work¹¹ this protein retained mineralization potential attributed to the BSP domain and sustained human mesenchymal stem cell proliferation and differentiation into the osteogenic lineage. However, if this protein is to be used for bone regeneration applications additional mechanical and structural studies were required. The force curves collected for the 6mer and 6mer+BSP films showed that the 6mer+BSP had a higher stiffness, likely due to the glutamic acid residues. Furthermore, the behaviour of the new recombinant protein in the presence of Ca, and as reported previously by others for osteopontin, amelogenin and dentin matrix protein, the present chimeric protein retained the ability to form supramolecular networks in the presence of Ca^{2+} ions through ionic cross-linking. This study shows the potential for new bioengineered polymers, such as 6mer+BSP, for the design of new nanocomposite systems. The presence of the silk domain in 6mer+BSP protein allows this biopolymer to be processed into different three-dimensional scaffolds. In addition, the BSP domain with its Ca affinity provides functions as an organic glue for use in new synthetic nanoscale composites, cross-linking organic and inorganic components, such as hydroxyapatite crystals, and increasing the stiffness and toughness of these systems by dissipating energy through the break of sacrificial bonds.

Acknowledgments

Silvia Gomes thanks the Foundation for Science and Technology (FCT) for supporting her PhD grant, SFRH/BD/28603/2006. This work was carried out under the scope of the European NoE EXPERTISSUES (NMP3-CT-2004-500283), the Chimera project (PTDC/EBB-EBI/109093/2008) funded by the FCT agency, the NIH (P41 EB002520) Tissue Engineering Resource Center and the NIH (EB003210 and DE017207).

References

1. Scheibel T. *Microb Cell Fact.* 2004; 3:14–24. [PubMed: 15546497]
2. Foo CWP, Bini E, Huang J, Lee SY, Kaplan DL. *Appl Phys Mater Sci Process.* 2006; 82:193–203.
3. Hayashi CY, Shipley NH, Lewis RV. *Int J Biol Macromol.* 1999; 24:271–275. [PubMed: 10342774]
4. Beek, JDv; Hess, S.; Vollrath, F.; Meier, BH. *Proc Natl Acad Sci USA.* 2002; 99:10266–10271. [PubMed: 12149440]
5. Altman GH, Diaz F, Jakuba C, Calabro T, Horan RL, Chen J, Lu H, Richmond J, Kaplan DL. *Biomaterials.* 2003; 24:401–416. [PubMed: 12423595]
6. Gosline J, Lillie M, Carrington E, Guerette P, Ortlepp C, Savage K. *Philos Trans R Soc Lond B Biol Sci.* 2002; 357:121–132. [PubMed: 11911769]
7. Wall JC, Chatterji SK, Jeffery JW. *Calcif Tissue Int.* 1979; 27:105–108. [PubMed: 110411]
8. Stark M, Grip S, Rising A, Hedhammar M, Engström W, Hjälm G, Johansson J. *Biomacromolecules.* 2007; 8:1695–1701. [PubMed: 17402782]
9. Oroudjev E, Soares J, Arcidiacono S, Thompson JB, Fossey SA, Hansma HG. *Proc Natl Acad Sci USA.* 2002; 99:6460–6465. [PubMed: 11959907]

10. Rabotyagova O, Cebe P, Kaplan DL. *Biomacromolecules*. 2009; 10:229–236. [PubMed: 19128057]
11. Gomes S, Leonor IB, Mano JF, Reis RL, Kaplan DL. *Soft Matter*. 2010 Submitted.
12. Baht GS, Hunter GK, Goldberg HA. *Matrix Biology*. 2008; 27:600–608. [PubMed: 18620053]
13. Mizuno M, Imai T, Fujisawa R, Tani H, Kuboki Y. *Calcif Tissue Int*. 2000; 66:388–396. [PubMed: 10773110]
14. Valverde P, Zhang J, Fix A, Zhu J, Ma W, Tu Q, Chen J. *J Bone Miner Res*. 2008; 23:1775–1778. [PubMed: 18597627]
15. Domke J, Radmacher M. *Langmuir*. 1998; 14:3320–3325.
16. Schäfer A, Vehoff T, Glisovič A, Salditt T. *Eur Biophys J*. 2008; 37:197–204. [PubMed: 17851658]
17. Ganss B, Kim RH, Sodek J. *Crit Rev Oral Biol Med*. 1999; 10:79–98. [PubMed: 10759428]
18. Goldberg H, Warner K, Li M, Hunter G. *Connect Tissue Res*. 2001; 42:25–37. [PubMed: 11696986]
19. Fantner GE, Adams J, Turner P, Thurner PJ, Fisher LW, Hansma PK. *Nano Lett*. 2007; 7:2491–2498. [PubMed: 17645366]
20. He G, Dahl T, Veis A, George A. *Connect Tissue Res*. 2003; 44:240–245. [PubMed: 12952204]
21. Kowalewski T, Holtzman DM. *Proc Natl Acad Sci USA*. 1999; 96:3688–3693. [PubMed: 10097098]
22. Cacciafesta P, Hallam KR, Watkinson AC, Allen GC, Miles MJ, Jandt KD. *Surf Sci*. 2001; 491:405–420.
23. Gadelmawla ES, Koura MM, Maksoud TMA, Elewa IM, Soliman HH. *J Mater Process Technol*. 2002; 123:133–145.
24. Johnson, KL. *Contact mechanics*. Cambridge University Press; Cambridge: 1994.
25. Sneddon IN. *Int J Eng Sci*. 1965; 3:47–57.
26. Schäfer A, Vehoff T, Glišovič A, Salditt T. *European Biophysics Journal*. 2008; 37:197–204. [PubMed: 17851658]
27. Radmacher M, Fritz M, Kacher CM, Cleveland JP, Hansma PK. *Biophys J*. 1996; 70:556–567. [PubMed: 8770233]
28. Wagh AA, Roan E, Chapman KE, Desai LP, Rendon DA, Eckstein EC, Waters CM. *Am J Physiol Lung Cell Mol Physiol*. 2008; 295:L54–L60. [PubMed: 18487359]
29. Hu X, Kaplan D, Cebe P. *Macromolecules*. 2006; 39:6161–6170.
30. Arrondo J, Goñi F. *Prog Biophys Mol Biol*. 1999; 72:367–405. [PubMed: 10605294]
31. Rabotyagova OS, Cebe P, Kaplan DL. *Macromol Biosci*. 2010; 10:49–59. [PubMed: 19890885]
32. Cerpa R, Cohen FE, Kuntz ID. *Fold Des*. 1996; 1:91–101. [PubMed: 9079369]
33. Kelly SM, Jess TJ, Price NC. *Biochim Biophys Acta*. 2005; 1751:119–139. [PubMed: 16027053]
34. Pérez-Rigueiro J, Viney C, Llorca J, Elices M. *Polymer*. 2000; 41:8433–8439.
35. Mano JF. *Macromol Biosci*. 2008; 8:69–76. [PubMed: 17902189]
36. Marsha RE, Coreya RB, Pauling L. *Biochim Biophys Acta*. 1955; 16:1–34. [PubMed: 14363226]
37. Fulara A, Dzwolak W. *J Phys Chem B*. 2010; 114:8278–8283. [PubMed: 20509699]
38. Zanuy D, Alemán C, Muñoz-Guerra S. *Int J Biol Macromol*. 1998; 23:175–184. [PubMed: 9777704]
39. Pérez-Rigueiro J, Viney C, Llorca J, Elices M. *Polymer*. 2000; 41:8433–8439.
40. Yin J, Chen E, Porter D, Shao Z. *Biomacromolecules*. 2010.1021/bm100643q
41. Gosline JM, Guerette PA, Ortlepp CS, Savage KN. *J Exp Biol*. 1999; 202:3295–3303. [PubMed: 10562512]
42. Becker N, Oroudjev E, Mutz S, Cleveland JP, Hansma PK, Hayashi CY, Makarov DE, Hansma HG. *Nat Mater*. 2003; 2:278–283. [PubMed: 12690403]
43. Smith BL, Schäffer TE, Viani M, Thompson JB, Frederick NA, Kindt J, Belcher A, Stucky GD, Morse DE, Hansma PK. *Nature*. 1999; 399:761–763.

44. Boussu K, Bruggen Vd, Volodin A, Snauwaert J, Haesendonck CV, Vandecasteele C. *J Colloid Interface Sci.* 2005; 286:632–638. [PubMed: 15897082]
45. Koinkar VN, Bhushan B. *J Appl Phys.* 1997; 81:2472–2479.
46. Poon CY, Bhushan B. *Wear.* 1995; 190:76–88.
47. Poon CY, Bhushan B. *Wear.* 1995; 190:89–109.
48. Sedin DL, Rowlen KL. *Appl Surf Sci.* 2001; 182:40–48.
49. Huang HH, Ho CT, Lee TH, Leec TL, Liao KK, Chen FL. *Biomol Eng.* 2004; 21:93–97. [PubMed: 15567102]
50. Lincks J, Boyan BD, Blanchard R, Lohmann CH, Liu Y, Cochran DL, Dean DD, Schwartz Z. *Biomaterials.* 1998; 19:2219–2232. [PubMed: 9884063]
51. Zinger O, Anselme K, Denzer A, Habersetzer P, Wieland M, Jeanfils J, Hardouin P, Landolta D. *Biomaterials.* 2004; 25:2695–2711. [PubMed: 14962549]
52. Wu Y, Zitelli JP, TenHuisen KS, Yu X, Libera MR. *Biomaterials.* 2011; 32:951–960. [PubMed: 20974493]
53. Chauvy PF, Madore C, Landolt D. *Surf Coat Technol.* 1998; 110:48–56.
54. Jackson AP, Vincenta JFV, Turner RM. *Compos Sci Technol.* 1989; 36:255–266.
55. Weiner S. *Crit Rev Biochem Mol Biol.* 1986; 20:365–408.
56. Thompson JB, Kindt JH, Drake B, Hansma HG, Morse DE, Hansma PK. *Nature.* 2001:414. [PubMed: 11473310]
57. Sun C, Fantner GE, Adams J, Hansma PK, Waite JH. *J Exp Biol.* 2007; 210:1481–1488. [PubMed: 17401131]
58. Kroger N, Bergsdorf C, Sumper M. *EMBO.* 1994; 13:4676–4683.
59. Currey J. *Nature.* 2001; 414:699. [PubMed: 11742376]
60. Fantner GE, Hassenkam T, Kindt JH, Weaver JC, Birkedal H, Pechenik L, Cutroni JA, Cidade GAG, Stucky GD, Morse DE, Hansma PK. *Nat Mater.* 2005; 4:612–616. [PubMed: 16025123]
61. Gupta HS, Fratzl P, Kerschnitzki M, Benecke G, Wagermaier W, Kirchner HOK. *J R Soc Interface.* 2007; 4:277–282. [PubMed: 17251154]
62. Gupta HS, Wagermaier W, Zickler GA, Aroush DR-B, Funari SS, Roschger P, Wagner HD, Fratzl P. *Nano Lett.* 2005; 5:2108–2111. [PubMed: 16218747]
63. Hansma PK, Fantner GE, Kindt JH, Thurner PJ, Schitter G, Turner PJ, Udwin SF, Finch MM. *J Musculoskelet Neuronal Interact.* 2005; 5:313–315. [PubMed: 16340118]
64. Fincham AG, Moradian-Oldak J, Simmer JP, Sarte P, Lau EC, Diekwisch T, Slavkin HC. *J Struct Biol.* 1994; 112:103–109. [PubMed: 8060728]
65. Adams J, Fantner GE, Fisher LW, Hansma PK. *Nanotechnology.* 2008; 19:384008–384015. [PubMed: 18843380]
66. Williams, RJP. A general introduction to the special properties of the calcium ion and their deployment in biology. In: Siegel, FL.; Carafoli, E.; Kretsinger, RH.; MacLennan, DH.; Wasserman, R., editors. *Calcium Binding Proteins: Structure and Function.* Elsevier North Holland Inc; NY: 1980.
67. Yamada K, Tsuboi Y, Itaya A. *Thin Solid Films.* 2003; 440:208–216.
68. Hossain KS, Nemoto N. *Langmuir.* 1999; 15:4114–4119.
69. Yang Y, Cui Q, Sahai N. *Langmuir.* 2010; 26:9848–9859. [PubMed: 20438109]
70. Alonso DOV, Daggett V. *J Mol Biol.* 1995; 247:501–520. [PubMed: 7714903]
71. Schiffer CA, Dötsch V. *Curr Opin Biotechnol.* 1996; 7:428–432. [PubMed: 8768902]
72. Tang Z, Kotov NA, Magonov S, Ozturk B. *Nat Mater.* 2003; 2:413–418. [PubMed: 12764359]

SGRGGLGGQGAGAAAAAGGAGQGGYGGGLGSQGTSGRG
 GLGGQGAGAAAAAGGAGQGGYGGGLGSQGTSGRGGLGG
 QGAGAAAAAGGAGQGGYGGGLGSQGTSGRGGLGGQGAG
 AAAAAGGAGQGGYGGGLGSQGTSGRGGLGGQGAGAAAA
 AGGAGQGGYGGGLGSQGTSGRGGLGGQGAGAAAAAGGA
 GQGGYGGGLGSQGTWPSRPTMKTALILLSILGMACAFSM
 KNLHRRVKIEDSEENGVFKYRPRYYLYKHAYFYPHLKRFP
 VQGSSDSSEENGDDSSSEEEEEEEETSNEGENNEESNED
 EDSEAENTTLSATTLGYGEDATPGTGTYGLAAIQLPKKAG
 DITNKATKEKESDEEEEEEEEGNENESEAEVDENEQGIN
 GTSTNSTEAENGNSSGGDNGEEGEEESVTGANAEGTT
 ETGGQGKGTSKTTTSPNGGFEP TTPPQVYRTTSPFGKT
 TTVEYEGEYETGVNEYDNGYEIYESENGEPRGDNYRAY
 EDEYSYFKGQGYDGYDGQNYHHQGLMGH Stop

Figure 1. Amino acid sequence for the 6mer+BSP protein. The linkers for the BSP sequence are underlined. The 6mer is represented in black and the BSP sequence is represented in gray.

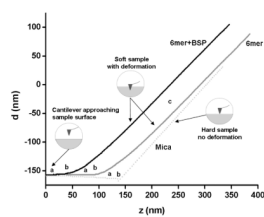


Figure 2. Force curves on 6mer and 6mer+BSP films, and on mica: a) cantilever approaching the surface; b) contact point; c) cantilever in contact with the surface.

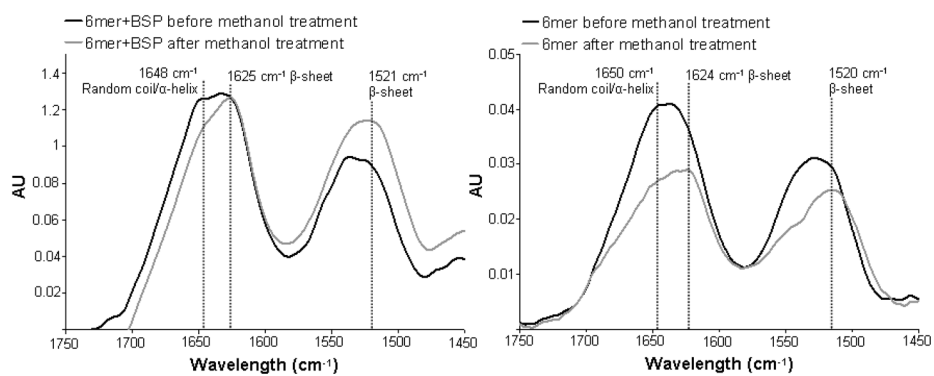


Figure 3. ATR-FTIR spectra of the 6mer and 6mer+BSP films after 2 hours of treatment with 70% methanol.

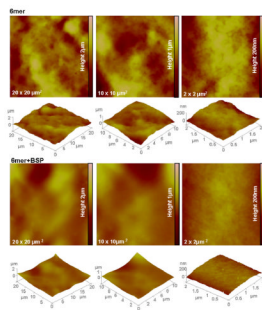


Figure 4. Topographies of AFM images (tapping mode) for 2% 6mer and 6mer+BSP films using $20 \times 20 \mu\text{m}^2$, $10 \times 10 \mu\text{m}^2$ and $2 \times 2 \mu\text{m}^2$ scan sizes.

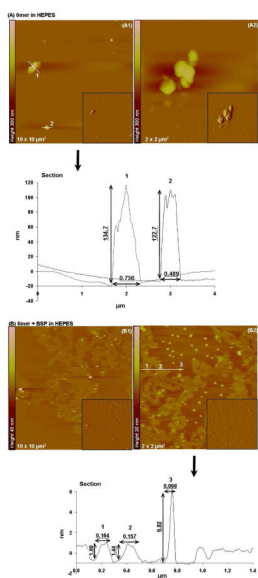


Figure 5. Topographies of AFM images (tapping mode) and corresponding section analysis of 6mer (A1–A2) and 6mer+BSP (B1–B2,) proteins in HEPES buffer 0.1 mM (pH 7.4).

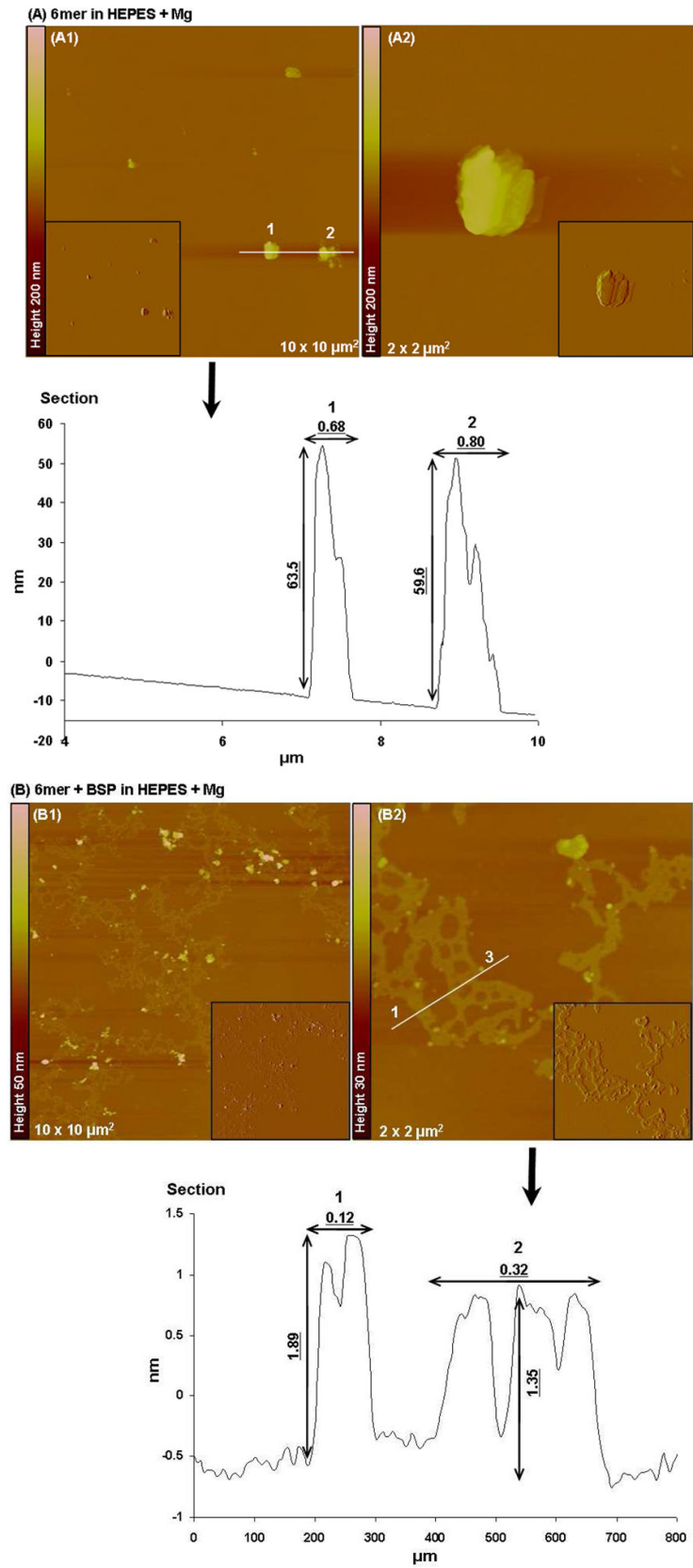
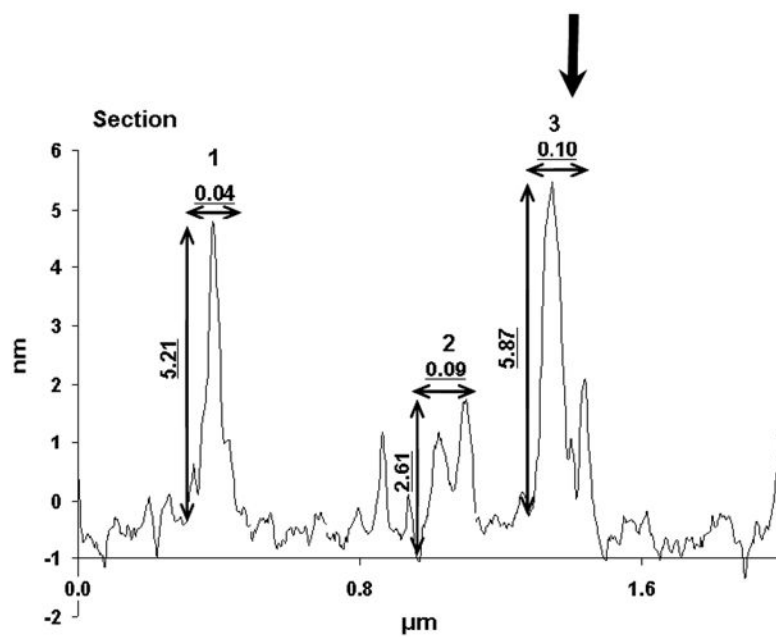
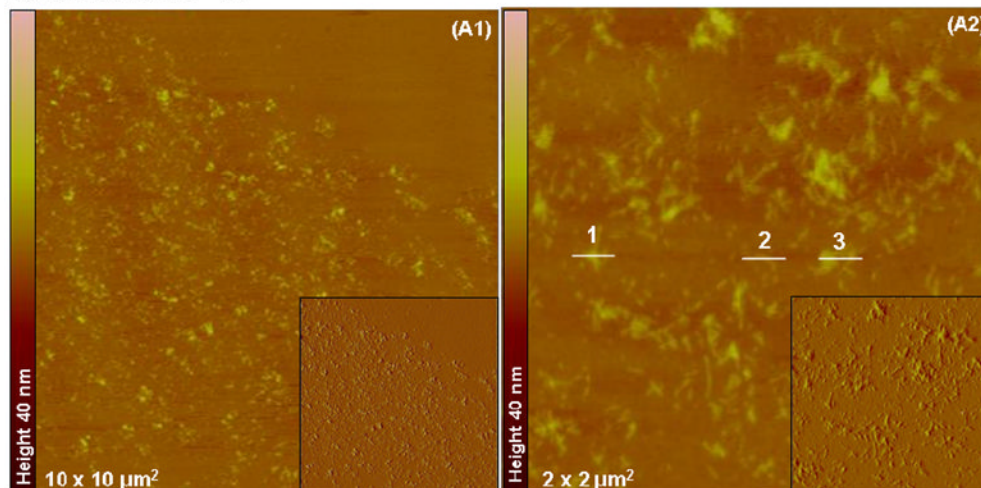


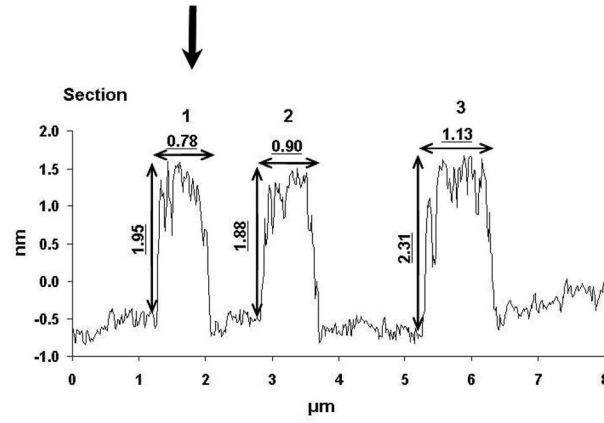
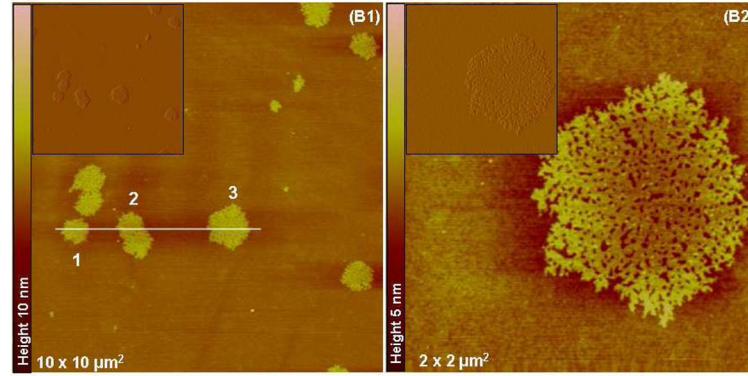
Figure 6.

Topographies AFM images (tapping mode) and corresponding section analysis of 6mer (A1–A2) and 6mer+BSP (B1–B2) proteins in HEPES buffer 0.1 mM with Mg in a ratio of 1:1000 (protein:Mg).

(A) 6mer in HEPES + Ca



(B) 6mer + BSP in HEPES + Ca



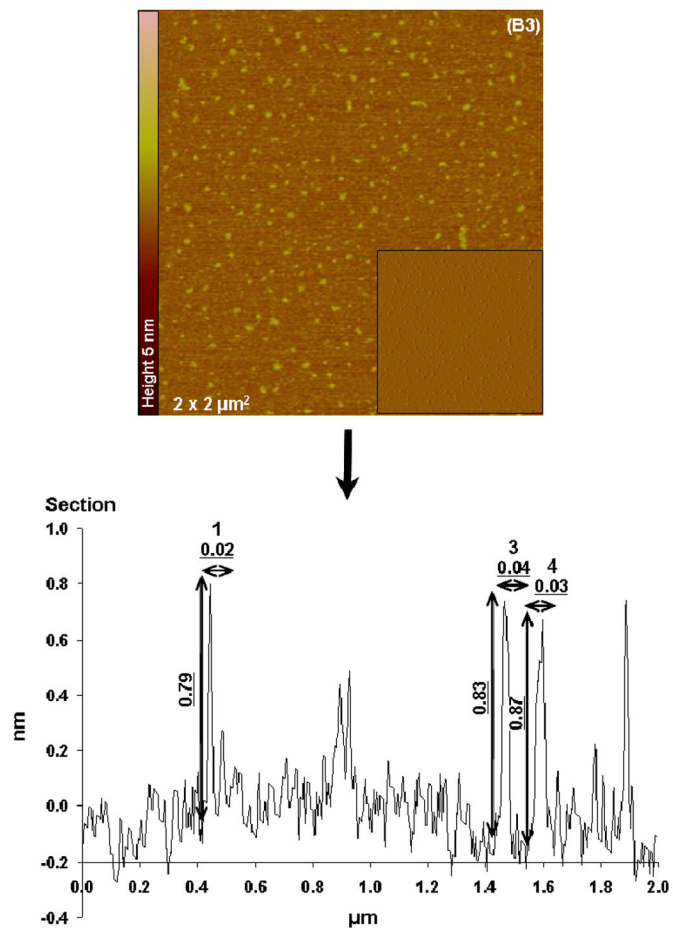


Figure 7. Topographies AFM images (tapping mode) and corresponding section analysis of 6mer (A1–A2) and 6mer+BSP (B1–B3) proteins in HEPES buffer 0.1 mM with Ca in a ratio of 1:1000 (protein:Ca).

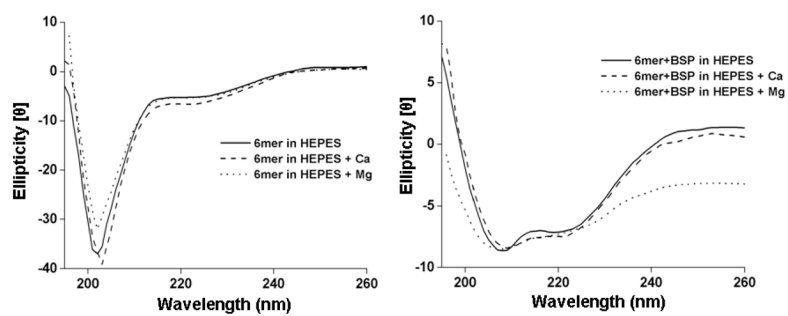


Figure 8. CD spectra for the 6mer and 6mer+BSP recombinant proteins dissolved in HEPES buffer 0.1 mM (pH 7.4), in HEPES buffer 0.1 mM with Ca in a ratio of 1:1000 (protein:Ca) and in HEPES buffer 0.1 mM with Mg in a ratio of 1:1000 (protein:Mg).

Table 1

Percentage of β -sheet and helix/random coil for 6mer control and 6mer+BSP films after methanol treatment.

Sample	β -sheet	Random coil/ α -helix
6mer	34.5 \pm 6	31.3 \pm 7
6mer+BSP	34.3 \pm 3	33.4 \pm 9

Table 2

Surface roughness, RMS and R_a for the 6mer and 6mer+BSP films using different scan sizes.

	6mer			6mer+BSP			Mica		
	RMS(nm)	R_a (nm)	RMS(nm)	R_a (nm)	RMS(nm)	R_a (nm)	RMS(nm)	R_a (nm)	
$20 \times 20 \mu\text{m}^2$ scan size	252.8 ± 43.2	194.2 ± 32.0	249.4 ± 70.4	201.8 ± 61.4	0.881	0.712			
$10 \times 10 \mu\text{m}^2$ scan size	124.4 ± 11	99.6 ± 8.8	144.8 ± 79.1	115.1 ± 63.0	0.455	0.377			
$2 \times 2 \mu\text{m}^2$ scan size	23 ± 5.1	18.3 ± 4.8	14.6 ± 6.0	12.2 ± 5.5	0.084	0.066			

RMS - root mean square; R_a - arithmetic average height